JAERI-M
87-211

RF HEATING AND CURRENT DRIVE EXPERIMENTS ON JT-60

January 1988

Kazuya UEHARA, Yoshitaka IKEDA, Mikio SAIGUSA, Keishi SAKAMOTO
Tsuneyuki FUJII, Kenkichi USHIGUSA, Sunao MAEBARA, Masaki TSUNEOKA
Masami SEKI, Shinichi MORIYAMA, Noriyuki KOBAYASHI, Tsuyoshi IMAI
Haruyuki KIMURA, Takashi NAGASHIMA and JT-60 Team

日本原子力研究所
Japan Atomic Energy Research Institute

JAERI-M 87-211　ERRATA

Page	line	wrong	right
(1)	5	Norkiyuki	Noriyuki
(3)	15	…のＲＦパのーを	…のＲＦパワーを
(6)	9	…に開ける…	…に於ける…
5	16	・・・m=1 mode	・・・m=2 mode
6	6	of X_e is	of χ_e is
6	7	・・・X_e =	・・・χ_e =

JAERI-M レポートは、日本原子力研究所が不定期に公刊している研究報告書です。
本書の問合せ先は、日本原子力研究所技術情報部情報資料課（〒319-11 茨城県那珂郡東海村）あて、お申しこしください。なお、このほかに財団法人原子力弘済会資料センター（〒319-11 茨城県那珂郡東海村日本原子力研究所内）で複写による実費頒布をおこなっております。

JAERI-M reports are issued irregularly.
Inquiries about availability of the reports should be addressed to Information Division, Department of Technical Information, Japan Atomic Energy Research Institute, Tokai-mura, Naka-gun, Ibaraki-ken 319-11, Japan.

JAERI-M 87-211

RF Heating and Current Drive Experiments on JT-60

Kazuya UEHARA, Yoshitaka IKEDA, Mikio SAIGUSA
Keishi SAKAMOTO, Tsuneyuki FUJII, Kenkichi USHIGUSA
Sunao MAEBARA, Masaki TSUNEOKA, Masami SEKI,
Shinichi MORIYAMA, Noriyuki KOBAYASHI, Tsuyoshi IMAI
Haruyuki KIMURA, Takashi NAGASHIMA and JT-60 Team

Department of JT-60 Facility
Department of Large Tokamak Research
Department of Thermonuclear Fusion Research
Naka Fusion Research Establishment
Japan Atomic Energy Research Institute
Naka-machi, Naka-gun, Ibaraki-ken

(Received December 17, 1987)

Recent experimental results of Lower Hubrid and Ion Cyclotron Range of Frequencies (LHRF and ICRF) heating and current drive are presented on JT-60 at JAERI. About 24 MW LHRF at 2 GHz and 6 MW ICRF at 120 MHz system are installed in JT-60. LHRF has launched 11.0 MW and ICRF has launched 2.1 MW of rf power into the JT-60 plasma through the sufficient aging process of the power injection into the TDC plasma and/or the vacuum chamber keeping 150°C baking of the launcher. Effective electron heating is performed with LHRF and with the combination of NBI and LHRF. Steady current drive of 2 MA for 2.5 sec and the current drive efficiency of $\eta_{CD} = (1.5\text{-}3.0) \times 10^{19}$ $m^{-2}AW^{-1}$ are obtained with and without NBI. Current ramp-up saves the volt·sec of OH transformer, which supports the high plasma current formation of 3.25 MA. Improvement of the plasma confinement at the low density region in LHCD is discussed including the pinch effect. Optimization of $2\,\omega_{ci}$ ICRF heating is studied with 2 × 2 phased loop antenna. Effective matching technique using movable stub tuner with high speed enable to quicken the aging process of ICRF power injection in JT-60 plasma. The phasing of $(\pi,0)$ of the loop antenna brings an effective power deposition into plasmas and the beam accelaration of NBI by ICRF wave was observed although the coupling resistance is relatively lower than the one of (0,0) mode. The beam

acceleration causes the relatively higher incremental energy confinement time of more than 200 msec, which is explained by the slowing down process of the accelerated ion tail.

Keywords: Lower-hybrid, Ion-cyclotron, Aging, Launcher, Current Drive, Current Ramp-up, Coupling Resistance, Beam Acceleration, Incremental Energy Confinement Time

ＪＴ－６０に於けるＲＦ加熱および電流駆動実験

日本原子力研究所那珂研究所
ＪＴ－６０試験部・臨界プラズマ研究部・核融合研究部
上原　和也・池田　佳隆・三枝　幹雄
坂本　慶司・藤井　常幸・牛草　健吉
前原　　直・恒岡まさき・関　　正美
森山　伸一・小林　則幸・今井　　剛
木村　晴行・永島　　孝・ＪＴ－６０チーム

（１９８７年１２月１７日受理）

最近の原研ＪＴ－６０に於ける低域混成波（Lover Hybrid Range of Frequency,LHRF）及びイオンサイクロトロン波（Ion Cyclotron Range of Frequency，ＩＣＲＦ）加熱実験及び電流駆動実験結果が示されている。ＪＴ－６０では2GHz帯２4MW出力のＬＨＲＦ加熱装置と１２０MHz帯6MW出力のICRF加熱装置のシステムが装備されており，ランチャーを１５０℃のベーキング状態に保ったまま，真空状態及びTDCプラズマへのＲＦパワーの入射という充分なエージング過程を経た上でＬＨＲＦは１１.０ＭＷ　ＩＣＲＦは2.1ＭＷ　のＲＦパのーをＪＴ－６０プラズマへ入射することに成功した。効果的な電子加熱がＬＨＲＦ及びＬＨＲＦとＮＢＩとの組み合わせの両方に於いて達成された。2.5秒間2MAのプラズマ電流をrf電流駆動によって達成し，LHRF及びLHRFとNBIとの同時入射によって電流駆動効率 $\eta_{CD}=(1.5-3.0)\times10^{19}\,m^{-2}AW^{-1}$ という値が得られた。電流点火によってＯＨ変圧器のボルト秒を節約し，３.２５ＭＡのプラズマ電流の生成を支えた。電流駆動時の低密度領域での閉じ込め時間の改善という現象がピンチ効果を含んで議論された。２×２位相制御型ループアンテナを用いた$2\omega ci$ＩＣＲＦ加熱実験が研究された。高速可動可能なスタブチューナを用いて整合する方法はＩＣＲＦパワーとＪＴ－６０プラズマとのエージング過程を速めることを可能にした。ループアンテナの（π，０）位相は（0,0）位相に比べて結合インピーダンスが比較的低いにもかかわらずプラズマへの効果的なパワー吸収をもたらし，同時にＩＣＲＦ波によるＮＢＩの顕者なビーム加速が観測された。このビーム加速は２００mse以上の比較的大きなエネルギー閉じ込め時間をもたらしており，これはＩＣＲＦによって加速されたＮＢＩのイオン・ティルの減速過程によって説明できる。

那珂研究所：〒311－02 茨城県那珂郡那珂町大字向山 801－1

Contents

目　　次

1. Introudction

JT-60 is only machine among the four large tokamaks (TFTR, JET, T-15 and JT-60)[1] that the additional heating apparatus with high power of both RF and NBI is equipped in relatively early stage and the LHRF is stressed to first priority among the rf heating. As early as 1977, JAERI had obtained successful results on both LHRF and ICRF using JFT-2, DIVA and JFT-2M, which indicates the first success of ion heating[2] and current drive[3] by LHRF in JFT-2 and impurity control by ICRF in JFT-2M.[4]. With these background, 24 MW LHRF at about 2 GHz 6 MW ICRF at about 120 MHz for 10 s have been installed for the JT-60 additional heating, in which is included high power klystron with 1 MW development[5,6] and the real time feed back control capability of the phase difference, power and the frequency (LHRF) and stub tuner (ICRF), respectively. It is noted that the LHRF and ICRF power of 11.0 MW and 2.1 MW are injected into JT-60 plasma, which may be brought by the good maintenance of the hardware and an optimum design[7].

This paper presents recent experimental results on LHRF and ICRF heating. In LHRF, the aging method of the launcher, electron heating with and without NBI, current drive and the interpretation of the improvement of the plasma confinement in LHCD are shown. In ICRF, the coupling properties of the 2 × 2 loop antenna array, the comparison on the experiment between (0,0) and (π,0) phasing and the beam acceleration by ICRF are shown.

2. System description[7]

JT-60 is an outside poloidal divertor tokamak with major and minor radii of 3 m and 0.93 m, respectively. Material of first wall is changed from TiC coated molibdenium to carbon graphite to supress the impurity level and about 300°C baking of the first wall are kept during discharge. JT-60 presently operates at plasma current up to I_p = 2.7 MA with divertor and I_p = 3.25 MA with limiter supported by the saving volt·sec due to LHCD. Experiments described in this paper were performed in the hydrogen or helium plasma in the range of $\bar{n}_e = (0.2\text{-}11.2) \times 10^{19}$ m^{-3}, $I_p \leqq 3.25$ MA, $B_t \leqq 4.8$ T and q_{eff} = 2-11, respectively.

In JT-60, 20 MW NBI and 10 MW RF deposition into plasma can be expected as an additional heating power. NBI heating system is composed of 28 beam lines in 14 units and has total injection power of 20 MW with hydrogen beam energy of 40 - 75 keV. RF heating system is composed of 4 units correspond-

1. Introudction

JT-60 is only machine among the four large tokamaks (TFTR, JET, T-15 and JT-60)[1] that the additional heating apparatus with high power of both RF and NBI is equipped in relatively early stage and the LHRF is stressed to first priority among the rf heating. As early as 1977, JAERI had obtained successful results on both LHRF and ICRF using JFT-2, DIVA and JFT-2M, which indicates the first success of ion heating[2] and current drive[3] by LHRF in JFT-2 and impurity control by ICRF in JFT-2M.[4]. With these background, 24 MW LHRF at about 2 GHz 6 MW ICRF at about 120 MHz for 10 s have been installed for the JT-60 additional heating, in which is included high power klystron with 1 MW development[5,6] and the real time feed back control capability of the phase difference, power and the frequency (LHRF) and stub tuner (ICRF), respectively. It is noted that the LHRF and ICRF power of 11.0 MW and 2.1 MW are injected into JT-60 plasma, which may be brought by the good maintenance of the hardware and an optimum design[7].

This paper presents recent experimental results on LHRF and ICRF heating. In LHRF, the aging method of the launcher, electron heating with and without NBI, current drive and the interpretation of the improvement of the plasma confinement in LHCD are shown. In ICRF, the coupling properties of the 2 × 2 loop antenna array, the comparison on the experiment between (0,0) and (π,0) phasing and the beam acceleration by ICRF are shown.

2. System description[7]

JT-60 is an outside poloidal divertor tokamak with major and minor radii of 3 m and 0.93 m, respectively. Material of first wall is changed from TiC coated molibdenium to carbon graphite to supress the impurity level and about 300°C baking of the first wall are kept during discharge. JT-60 presently operates at plasma current up to I_p = 2.7 MA with divertor and I_p = 3.25 MA with limiter supported by the saving volt·sec due to LHCD. Experiments described in this paper were performed in the hydrogen or helium plasma in the range of $\bar{n}_e = (0.2\text{-}11.2) \times 10^{19}$ m^{-3}, $I_p \leq 3.25$ MA, $B_t \leq 4.8$ T and q_{eff} = 2-11, respectively.

In JT-60, 20 MW NBI and 10 MW RF deposition into plasma can be expected as an additional heating power. NBI heating system is composed of 28 beam lines in 14 units and has total injection power of 20 MW with hydrogen beam energy of 40 - 75 keV. RF heating system is composed of 4 units correspond-

ing to injection ports. One of the most remarkable characteristics in JT-60 LHRF launchers is that the vacuum windows are located far away from the plasma (6 m), which is designed for the efficient aging of launcher evaluating the accumulated data of JFT-2[8] and the RF teststand RFTS-I and II in JAERI[9].

LHRF heating system has 3 units. Each unit has 8 MW RF generators with 8 klystrons of 1 MW at a frequency of 2 GHz. The LHRF waves are launched by three 4 × 8 waveguides coupler. One of these grills is designed for the current drive of small width waveguide with a n_z index of 1.7 for a phasing $\Delta\phi = 90°$ and the other two grills for the heating of large width waveguide with a n_z of ± 1.8 for $\Delta\phi = 180°$. One of more excellent characteristics of LHRF heating system is that 24 klystrons with 1 MW per one tube are stably operating without any output circulators to protect klystrons against the large refrective power from the plasma.

ICRF heating system has 1 unit. This unit has 6 MW generators with 8 tetrodes of 750 KW at a frequency of 120 MHz. The ICRF wave are launched by 2 × 2 loop antenna coupler, which has been developed for the optimization of the second hamonic heating of hydrogen plasmas and the phase control of both toroidal and poloidal direction.

The total RF heating system is remotely controlled via mini-computer, which is linked with "ZENKEI" the central control system of JT-60 and the "CAMAC" system. The main parameters (rf power P_{rf}, phase difference in adjascent waveguide $\Delta\phi$, frequency f (LHRF) and the position of stub tuner (ICRF), which is preprogram control) are linked with the Dual Port Memory with D-port(DPMP) of ZENKEI via high speed CAMAC system and are feed back controlled in a real time so as to respond to fast varying plasma paramers during rf injection[10,11].

3. LHRF results

3.1 Coupling properties[12]

Size of each element is 1.6 cm × 11.5 cm and 2.9 cm × 11.5 cm for LHCD and LHH, respectively. Aging process must be sufficiently artificially in order to get much rf power injection into plasma. Since the vacuum window is far from plasma, the vacuum technology during rf injection is a frontier in JT-60 aging technique. For example, carbon is coated on the copper surface of waveguide in the area where the frequency of 2 GHz corresponds to the second hamonic electron cyclotron resonance due to the residual

ing to injection ports. One of the most remarkable characteristics in JT-60 LHRF launchers is that the vacuum windows are located far away from the plasma (6 m), which is designed for the efficient aging of launcher evaluating the accumulated data of JFT-2[8] and the RF teststand RFTS-I and II in JAERI[9].

LHRF heating system has 3 units. Each unit has 8 MW RF generators with 8 klystrons of 1 MW at a frequency of 2 GHz. The LHRF waves are launched by three 4 × 8 waveguides coupler. One of these grills is designed for the current drive of small width waveguide with a n_z index of 1.7 for a phasing $\Delta\phi = 90°$ and the other two grills for the heating of large width waveguide with a n_z of ± 1.8 for $\Delta\phi = 180°$. One of more excellent characteristics of LHRF heating system is that 24 klystrons with 1 MW per one tube are stably operating without any output circulators to protect klystrons against the large refrective power from the plasma.

ICRF heating system has 1 unit. This unit has 6 MW generators with 8 tetrodes of 750 KW at a frequency of 120 MHz. The ICRF wave are launched by 2 × 2 loop antenna coupler, which has been developed for the optimization of the second hamonic heating of hydrogen plasmas and the phase control of both toroidal and poloidal direction.

The total RF heating system is remotely controlled via mini-computer, which is linked with "ZENKEI" the central control system of JT-60 and the "CAMAC" system. The main parameters (rf power P_{rf}, phase difference in adjascent waveguide $\Delta\phi$, frequency f (LHRF) and the position of stub tuner (ICRF), which is preprogram control) are linked with the Dual Port Memory with D-port(DPMP) of ZENKEI via high speed CAMAC system and are feed back controlled in a real time so as to respond to fast varying plasma paramers during rf injection[10,11].

3. LHRF results

3.1 Coupling properties[12]

Size of each element is 1.6 cm × 11.5 cm and 2.9 cm × 11.5 cm for LHCD and LHH, respectively. Aging process must be sufficiently artificially in order to get much rf power injection into plasma. Since the vacuum window is far from plasma, the vacuum technology during rf injection is a frontier in JT-60 aging technique. For example, carbon is coated on the copper surface of waveguide in the area where the frequency of 2 GHz corresponds to the second hamonic electron cyclotron resonance due to the residual

poloidal magnetic field, which is effective to suppress the break down due to the unipole multipactering discharge[13]. During the experiment we keep enough baking (~150°C) of lauching structure continuously. Before the injection to the main plasma the rf injection into vacuum chamber and also the rf injection to TDC plasma are performed. Wave pattern is much contrived for a sufficient aging using the method of pin (pulse) and AM modulation, which is shown in Fig. 1. After the above mentioned aging we performs about 3.4 MW in each unit and 11 MW injection in total, the history of which is shown in Fig. 2. The reflection coefficience is kept to below 20 % in each unit and the coupling efficiency depends on the distance between a coupler and a plasma edge as shown in Fig. 3. Here, a solid and a broken curve indicate Brambilla gril theory, if we consider the density gradient in front of launcher as

$$\nabla n_e = \frac{n_{es}}{\nabla L} \exp(-\Delta l/\lambda) \qquad (1)$$

where n_{es} is the density at the separatrix, Δl is the length between separatrix and limiter, ΔL is the length between limiter and launcher. Obtained power density in maximum is 6.4 kW/cm^2 and 3.4 kW/cm^2 for LHCD and LHH launcher, respectively. The power density does not agree with the scaling, $1 + 0.45f^2b$, presented by Tonon[14], where f is the frequency and b is the width of each waveguide.

3.2 Electron Heating

Electron heating experiment is performed with $\Delta\phi = 90°$ and $180°$ for the current drive and heating launcher, respectively. Figure 4 shows the electron temperature profile measured by Thomson scattering in OH disharge and LHEH ones by LHRF power injection of 2.4 MW, in which a maximum electron temperature is obtained in JT-60. The increment of the central electron temperature T_{e0} is shown against the absorption power P_{abs} normalizd by the average density $\bar{n}_e$ in Fig. 5, which indicates that the increment of T_{e0} in LHEH is larger than NBI and comparable to OH case at the region of $P_{abs}/\bar{n}_e < 3 \times 10^{-19}$ MW/m^3. The value of T_{e0} decreases with $\bar{n}_e$ and the ion temperature up to 1 keV is observed in this density region, while no high energy ion tail is observed. The stored energy W^* measured by diamagnetic loop is shown against P_{abs} in Fig. 6 putting the plasma current I_p as parameters, which indicates that W^* does not saturate at I_p = 2 MA case although W^* saturates at I_p = 1.5 MA case. In this case, the signal of hard X ray and

3 ω_{ce} electron cycrotron emission (ECE) does not further increase at P_{abs} > 6 MW and the H_{α} in the divertor room is enhanced at P_{abs} > 6 MW. The comparison with NBI case is shown in Fig. 7. The value of τ_E^{INC} for the LHEH case is 64 msec which is similar to NBI case (τ_E^{INC} = 60 msec) below 6 MW.

3.3 Combined LHRF and NBI

In order to expect the more deposition power into plasmas, we perform the simultaneous injection of LHRF and NBI. Typical data on the rf power, stored energy, average density, ion temperature by titanium XXI line T_I^{XXI} and active beam T_I^{AB} and emission by ECE are shown in Fig. 8. The stored energy reaches to about 1.7 MJ NBI of 19 MW and further increases about 270 kJ by LHRF of 4.7 MW and does not saturated at this density region ($\bar{n}_e < 4 \times 10^{19}$ cm^{-3}) as hown in Fig. 9. The incremental energy confinment time (=$\Delta W/\Delta P$) by LHRF decreases as $\bar{n}_e$ increases as shown in Fig. 10, while this value is almost constant (about 0.06 sec) for NBI alone case. It is noted that the production of the higher energy electron tail is different between LHRF case and the combination of LHEH and NBI case as shown in Fig. 11, which indicates that the count of hard X ray I_{HX} normalized by P_{LH} suddenly drops beyond $\bar{n}_e = 2.4 \times 10^{-19}$ m^{-3} although I_{HX}/P_{LH} extend to about $\bar{n}_e = 4 \quad 10^{-19}$ m^{-9} for LHEH alone case. This reduction must be compensated by the formation of higher energy ion tail by LHRF at the boundary region. In summary, the superposition effect by LHRF and NBI is obtained and in future the optimization of the phase difference must be tried.

3.4 Current drive, ramp-up and saving volt·sec

Current drive by LHRF must be most extensively performed to realize the steady state operation of tokamak reactor. In JT-60, 2 MA current drive at relatively low density region ($\bar{n}_e = 0.32 \times 10^{19}$ m^{-3}) is already succesful and the ramp-up as well as the saving of volt sec of OH transformer are obtained. The efficiency η_{CD} ($=\bar{n}_e R I_{rf}/P_{LH}$) is about (0.9 - 2.0) $\times 10^{19}$ m^{-2} A/W with LHRF alone, however, η_{CD} is improved to (1.5 - 3.0) $\times 10^{-19}$ m^{-2} A/W with the combination of NBI, which may be brought by the increment of the electron temperature. The optimum η_{CD} is obtained at $\Delta\phi = 90°$ for CD launcher and $\Delta\phi = 140°$ for heating launcher. The stored energy and pressure anisotropy of the superthermal electrons obtained by magnetic measurements indicates that the distribution function of the superthermal electrons modeled by a tree temperature Maxwellian with a flat tail is extending to the accessibility energy in the forward direction, a perpendicular

temperature of 150 keV, a backward parallel temperature of 250 keV, and a backward-to forward ratio of 2[15].

A typical shot of ramp-up is shown in Fig. 12. The plasma current was ramped up from 0.46 to 0.60 MA in 5.5 sec at $\bar{n}_e = 0.3 \times 10^{19}$ m^{-3} with P_{LH} = 1.6 MW. The ramp-up efficiency η_r is expressed as

$$\eta_r = (\dot{W}_{RF} - P_{ext} + V^2/R)/P_{LH} \qquad (2)$$

and is estimated to be η_r = 5.3 %, where poloidal field energy $\dot{W}_{RF} = d(LI_p^2/2)/dt$ is 67 kW, the external inductance power input P_{ext} is 2.5 kW and the resistive power loss V^2/R is 4.2 kW. This value is cosistent with typical medium size tokamak. The high plasma current formation of I_p = 3.25 MA to get more good confimenent plasma is performed by saving volt·sec due to LHRF ramp-up, which is shown in Fig. 13.

3.5 Discussion on the improvement of plasma confinement in LHCD

It is experimentally recognized that the energy confinement time in LHCD is improved at the low density region[17,18]. In this case, the suppression of sawteeth oscilation[19,20], the stabilization of m=1 mode[21]) and the broadening of the current profile are also observed. In JT-60, the improvement of τ_E is also observed at a relatively low density region ($\bar{n}_e < 1 \times 10^{19}$ m^{-3}) with the combination of NBI and LHCD[22]. It is probable that the internal inductance is reduced when τ_E is imporoved[23]. However, these phenomena does not connect directly to the explanation of the improvement of τ_E, because the current profile is independent on the temperature profile also from the standpoint of the profile consistency[24]. Possible explanation of this must be related to the reduction of the energy loss from the plasma core, especially such as a reduction of the electron thermal conductivity χ_e must be occured in the plasma core. As early as 1982, one of the authors (K.U.) has proposed the pinch effect in the LHCD as a reason of the improvement of the particle confinement time[25]. However, there had existed some problems in the theory whether the time averaged $E_z \times B_\theta$ drift does not really cancel out ? or how about is the $E_x \times B_z$ term ?, where E_z and E_x are the rf electric field in the toroidal and poloidal direction[26]. These problems are carefully considered on the standpoint of Landau damping in the presence of the magnetic field following Dawson like treatment[27] and in result it is obtained that $E_z \times B_\theta$ pinch term still remains in the LHCD and form a inward flux Γ_{pinch} as

$$\Gamma_{pinch} = \pm \frac{E_z^2 \omega_{c\theta}^{\pi}}{2B^2 k_z} \frac{df(v_z)}{dv_z}\Bigg|_{v_z=\omega/k_z} \tag{3}$$

where $\omega_{c\theta} = eB_\theta/m$, $B = \sqrt{B_z^2 + B_\theta^2}$ 16). The sign of - in R.H.S. of eq. (3) indicates the anti-current drive case. Assuming that the particle diffusion is reduced by this pinch effect as

$$-D \frac{\partial n_1}{\partial r} - \Gamma_{pinch} = -D_{eff} \frac{\partial n_2}{\partial r} \tag{4}$$

we can estimate the energy confinement time in LHCD. The value of x_e is improved by LHCD through the relation $x_e = \beta D_{eff}/\sqrt{q}$ and we assume the ion thermal conductivity to be neoclassical. Figure 14 is an example of the simulation in JT-60 LHCD with NBI, which indicates that τ_E does not detoriarate at a certain NBI power P_{NB}. Simulation shows that the key parameters are n_z and the electron temperature. In the case of Fig. 14, P_{NB} is the function on the electron temperature. Estimation of the pinch effect may support the fact in LHCD that the improvement in LHCD always accompany the improvement of the particle confiment time and the anticurrent drive does not bring the improvement of confiment[28] and also indicates that the travelling type electron heating is desirable for the improvement of the confiment.

4. ICRF results

4.1 Coupling properties[29,30]

The impedance of each antenna element is matched with 50 Ω transmission line by double stub tuner ($\lambda/4$ choke type). The stub tuners are electrically insulated from the launcher by DC breaks, whose rf leakage is kept below -90 dB. SF_6 gas in the feedthrough and stub tuner is circulated to bear the rf breakdown and to remove the rf joule loss. We employ two methods to get a impedance matching of antanna. One method is to move the stub tuner in preprogam with high speed of 25 mm/0.5 sec during plasma shot, in which we develop a choke planger type stub with bearing 1.5 MW power rating of VSWR of 25. We can find the optimum position of the stub tuner within several shots. Another method is to predict the optimum matching position of stub by using the experimental data of antenna input impedance. Figure 15 shows the time evolution of antenna impedance, $R_a + iX_a$, when the

$$\Gamma_{pinch} = \pm \frac{E_z^2 \omega_{c\theta}^{\pi}}{2B^2 k_z} \frac{df(v_z)}{dv_z} \Bigg|_{v_z=\omega/k_z} \tag{3}$$

where $\omega_{c\theta} = eB_\theta/m$, $B = \sqrt{B_z^2 + B_\theta^2}$ [16]. The sign of - in R.H.S. of eq. (3) indicates the anti-current drive case. Assuming that the particle diffusion is reduced by this pinch effect as

$$-D \frac{\partial n_1}{\partial r} - \Gamma_{pinch} = -D_{eff} \frac{\partial n_2}{\partial r} \tag{4}$$

we can estimate the energy confinement time in LHCD. The value of x_e is improved by LHCD through the relation $x_e = \beta D_{eff}/\sqrt{q}$ and we assume the ion thermal conductivity to be neoclassical. Figure 14 is an example of the simulation in JT-60 LHCD with NBI, which indicates that τ_E does not detoriarate at a certain NBI power P_{NB}. Simulation shows that the key parameters are n_z and the electron temperature. In the case of Fig. 14, P_{NB} is the function on the electron temperature. Estimation of the pinch effect may support the fact in LHCD that the improvement in LHCD always accompany the improvement of the particle confiment time and the anticurrent drive does not bring the improvement of confiment[28] and also indicates that the travelling type electron heating is desirable for the improvement of the confiment.

4. ICRF results

4.1 Coupling properties[29,30]

The impedance of each antenna element is matched with 50 Ω transmission line by double stub tuner (λ/4 choke type). The stub tuners are electrically insulated from the launcher by DC breaks, whose rf leakage is kept below -90 dB. SF_6 gas in the feedthrough and stub tuner is circulated to bear the rf breakdown and to remove the rf joule loss. We employ two methods to get a impedance matching of antanna. One method is to move the stub tuner in preprogam with high speed of 25 mm/0.5 sec during plasma shot, in which we develop a choke planger type stub with bearing 1.5 MW power rating of VSWR of 25. We can find the optimum position of the stub tuner within several shots. Another method is to predict the optimum matching position of stub by using the experimental data of antenna input impedance. Figure 15 shows the time evolution of antenna impedance, $R_a + iX_a$, when the

separatrix position is gradually shifted away from the antenna, where d is the distance from the Faraday shield to the separatrix. Using both methods above, we can get a good impedance match within a few shots as long as plasma is stable. We reach to the rf power injection of 2.1 MW (maximum power rating is 1.1 kW/cm^2 and the voltage in antenna is 45 kV in maximum) after the aging within several days.

The loading resistance versus $\bar{n}_e$ are shown in Fig. 16, where two curves are the theoretical one obtained by a three dimensional antenna-plasma coupling code and circles and triangles represent the experimental deta. The antenna loading resistance is about 5-10 Ω in (0,0) phasing and 2-3 Ω in (π,0) phasing. The cavity resonance mode is observed over a wide density region in (0,0) case, however, it is negligible except for the low density region in (π,0) case, which is supported by the theory.

4.2 Heating results with k_z phasing[31)]

The peak position of the k_z spectra of (0,0) and (π,0) modes are calculated to be 0 m^{-1} and 10 m^{-1}, respectively. It is shown experimentally in (0,0) phasing that the rise time of the plasma stored energy (Shafranov Λ ($=\beta_p + l_i/2 - 1$)) is small and τ_E^{INC} is 40 msec, indicating that the absorbed power in plasma core was very small. In (π,0) case, the rise time of Λ is very short and τ_E^{INC} is about 70 msec, which is comparable with NBI heating. Such large difference in the heating can be explained by the difference due to the power deposition profile. Figure 17 shows the Poynting vector in the poloidal cross section estimated by the two dimensional kinetic wave code[32)], which indicates that the heating power is directed to the center in (π,0) case, while the vecter is scattering in (0,0) case and in resultant to broaden the power deposition.

The radiation loss also depends on the phasing. In OH plasma with $\bar{n}_e = 6 \times 10^{19}$ m^{-3} and in the TiC coated wall, $\Delta P_{rad}/P_{IC}$ was about unity in (0,0) case but it decreases to 0.65 in (π,0) case, where ΔP_{rad} is the increment of the total radiation loss due to rf. Replacement of the first wall as well as the antenna guard limiter with carbon has brought the significant reduction of the radiation loss in both phasing.

4.3 Beam acceleration of NBI by ICRF

In combination heating with NBI and ICRF, we observe remakable beam acceleration further beyond the injection energy of NBI. It is shown experimentally that the increment of the beam energy spctra ΔT_i^{tail} is

proportional to the slowing down time $\tau_s (\propto T_e^{3/2}/\bar{n}_e)$ from $\bar{n}_e$-scan and $n_b \Delta T_i^{tail}/\tau_s$ ($\propto P_{IC}^b$, if the rf power deposition is coupled to the beam component, where P_{IC}^b is the ICRF power absorbed by the beam component) is proportional to the NBI power, where n_b is the density of the NBI beam component. Thereby, the rf power density absorbed by the beam component must be proportional to the beam power density. The efficiency of the acceleration (T_i^{tail}/P_{IC}) is 3.8 keV/MW in (π,0) and is about two times higher than in (0,0) at the same density ($3 - 4 \times 10^{19}$ m^{-3}). The effective increment of a stored energy is observed as shown in Fig. 18 including the electron temperature by electron cyclotron emission and the neutral flux with the charge exchange analyser with the energy of 68 keV and 103 keV. We can see that with the injection of 18 MW of NBI and 1.4 MW of ICRF W^* reaches 1.9 MJ and the increment by ICRF is 300 kJ. Sawteeth oscilation in the center is enhanced by ICRF but the high energy flux of 103 keV clearly increases by ICRF wave. Accompanying the beam acceleration, the increment of τ_E^{INC} is observed as shown in Fig. 19. The value of τ_E^{INC} increases with decrease of $\bar{n}_e$ and reaches to 210 msec, while τ_E^{INC} is about 50 msec with NBI alone.

5. Summary and conclusion

In summary, RF heating system with the capability of 24 MW LHRF and 6 MW ICRF are installed in JT-60. LHRF has launched 11.0 MW and ICRF 2.1 MW through the sufficient aging proccess such as high temperature baking of the launcher, rf injection with artificial wave pattern into vacuum and TDC plasma and so on. Electron heating bring high electron temperature of 6 keV and the stored energy of 0.9 MJ by LHRF and 2.3 MJ by NBI and LHRF are obtained at the low density region. Current drive brings the 2 MA of plasma current at the low density and the saving volt·sec is helpful to attain the high plasma current of 3.25 MA. Improvement of plasma confinement is discussed including the pinch effect. In ICRF, the matching technique of the phased 2 × 2 loop antenna array is established and the coupling properties of this coupler is clarified. The phasing of (π,0) of the loop antenna brings the effective power deposition into plasma and the remarkable beam acceleration of NBI although the coupling resistance is relatively lower. The beam acceleration causes the considerably higher incremental energy confinement of more than 200 msec, which is explained by the slowing down process of the accelerated ion tail.

proportional to the slowing down time $\tau_s (\propto T_e^{3/2}/\bar{n}_e)$ from $\bar{n}_e$-scan and $n_b \Delta T_i^{tail}/\tau_s$ ($\propto P_{IC}^b$, if the rf power deposition is coupled to the beam component, where P_{IC}^b is the ICRF power absorbed by the beam component) is proportional to the NBI power, where n_b is the density of the NBI beam component. Thereby, the rf power density absorbed by the beam component must be proportional to the beam power density. The efficiency of the acceleration (T_i^{tail}/P_{IC}) is 3.8 keV/MW in (π,0) and is about two times higher than in (0,0) at the same density ($3 - 4 \times 10^{19}$ m^{-3}). The effective increment of a stored energy is observed as shown in Fig. 18 including the electron temperature by electron cyclotron emission and the neutral flux with the charge exchange analyser with the energy of 68 keV and 103 keV. We can see that with the injection of 18 MW of NBI and 1.4 MW of ICRF W^* reaches 1.9 MJ and the increment by ICRF is 300 kJ. Sawteeth oscilation in the center is enhanced by ICRF but the high energy flux of 103 keV clearly increases by ICRF wave. Accompanying the beam acceleration, the increment of τ_E^{INC} is observed as shown in Fig. 19. The value of τ_E^{INC} increases with decrease of $\bar{n}_e$ and reaches to 210 msec, while τ_E^{INC} is about 50 msec with NBI alone.

5. Summary and conclusion

In summary, RF heating system with the capability of 24 MW LHRF and 6 MW ICRF are installed in JT-60. LHRF has launched 11.0 MW and ICRF 2.1 MW through the sufficient aging proccess such as high temperature baking of the launcher, rf injection with artificial wave pattern into vacuum and TDC plasma and so on. Electron heating bring high electron temperature of 6 keV and the stored energy of 0.9 MJ by LHRF and 2.3 MJ by NBI and LHRF are obtained at the low density region. Current drive brings the 2 MA of plasma current at the low density and the saving volt·sec is helpful to attain the high plasma current of 3.25 MA. Improvement of plasma confinement is discussed including the pinch effect. In ICRF, the matching technique of the phased 2 × 2 loop antenna array is established and the coupling properties of this coupler is clarified. The phasing of (π,0) of the loop antenna brings the effective power deposition into plasma and the remarkable beam acceleration of NBI although the coupling resistance is relatively lower. The beam acceleration causes the considerably higher incremental energy confinement of more than 200 msec, which is explained by the slowing down process of the accelerated ion tail.

Acknowledgements

The authors wish to thank the all members of JAERI who have contributed to the JT-60 project throughout its progress. They also wish to express their gratitude to Drs. S. Mori, Y. Iso, K. Tomabechi, H. Shirakata, M. Ohta and Y. Shimomura for continued encouragement and support.

References

1) A.H. Spano (compiler), Nucl. Fusion 15 (1975) 909.
2) T. Imai et al., Phys. Rev. Lett. 43 (1979) 586.
3) T. Yamamoto et al., Phys. Rev. Lett. 45 (1980) 716.
4) H. Tamai et al., Nucl. Fusion 26 (1986) 365.
5) S. Miyake et al., in Proc. IEEE Int. Electron devices Meeting, San Francisco, 1984.
6) Y. Kojima et al., in Proc. IEEE Int. Conf. on Plasma Sci., Pittsburg, 1985.
7) T. Nagashima and K. Uehara et al., Fusion Eng. Design 5 (1987) 101.
8) T. Fujii et al., Jpn. J. Appl. Phys. 22 (1983) 319.
9) T. Fujii et al., Proc. 3rd Varenna-Grenoble Int. Symp. Heating Toroidal Plasmas 3 (1982) 1133.
10) T. Fujii et al., in Proc. 12th Symp. Fusion Eng. Monterey, 1987.
11) K. Uehara et al., in Proc. 11th Symp. Fusion Eng. Austin, 1984, 1200.
12) Y. Ikeda et al., in Proc. 7th Topical Conf. RF heating, Florida, 1986.
13) K. Sakamoto et al., IEEE Trans. PS-14 (1986) 548.
14) G. Tonon, Plasma Phys. Contr. Fusion 28 (1984) 145.
15) Y. Takase et al., JAERI-M 87-200.
16) K. Uehara, JAERI-M 87-180, 1987.
17) F. Söldner et al., 13th European Conf. on Contr. Fusion & Plasma Phys., Schliersee, 1986, vol.II, p.343.
18) M. Porkolab et al., in Proc. 11th Int. Conf. Plasma Phys. Contr. Nucl. Fusion, IAEA-CN-F-II, Kyoto, 1986.
19) T.K. Chu et al., Nucl. Fusion 26 (1986) 666.
20) F.X. Söldner et al., Phys. Rev. Lett. 5 (1986) 1137.
21) D. Van Houtte et al., Nucl. Fusion 24 (1984) 1485.
22) JT-60 team, Proc. 11th Int. Conf. Plasma Phys. Contr. Fusion, IAEA-CN-K-I-1, Kyoto, 1986.
23) K. Ushigusa et al., JAERI M 87-012, 1987.

Acknowledgements

The authors wish to thank the all members of JAERI who have contributed to the JT-60 project throughout its progress. They also wish to express their gratitude to Drs. S. Mori, Y. Iso, K. Tomabechi, H. Shirakata, M. Ohta and Y. Shimomura for continued encouragement and support.

References

1) A.H. Spano (compiler), Nucl. Fusion 15 (1975) 909.
2) T. Imai et al., Phys. Rev. Lett. 43 (1979) 586.
3) T. Yamamoto et al., Phys. Rev. Lett. 45 (1980) 716.
4) H. Tamai et al., Nucl. Fusion 26 (1986) 365.
5) S. Miyake et al., in Proc. IEEE Int. Electron devices Meeting, San Francisco, 1984.
6) Y. Kojima et al., in Proc. IEEE Int. Conf. on Plasma Sci., Pittsburg, 1985.
7) T. Nagashima and K. Uehara et al., Fusion Eng. Design 5 (1987) 101.
8) T. Fujii et al., Jpn. J. Appl. Phys. 22 (1983) 319.
9) T. Fujii et al., Proc. 3rd Varenna-Grenoble Int. Symp. Heating Toroidal Plasmas 3 (1982) 1133.
10) T. Fujii et al., in Proc. 12th Symp. Fusion Eng. Monterey, 1987.
11) K. Uehara et al., in Proc. 11th Symp. Fusion Eng. Austin, 1984, 1200.
12) Y. Ikeda et al., in Proc. 7th Topical Conf. RF heating, Florida, 1986.
13) K. Sakamoto et al., IEEE Trans. PS-14 (1986) 548.
14) G. Tonon, Plasma Phys. Contr. Fusion 28 (1984) 145.
15) Y. Takase et al., JAERI-M 87-200.
16) K. Uehara, JAERI-M 87-180, 1987.
17) F. Söldner et al., 13th European Conf. on Contr. Fusion & Plasma Phys., Schliersee, 1986, vol.II, p.343.
18) M. Porkolab et al., in Proc. 11th Int. Conf. Plasma Phys. Contr. Nucl. Fusion, IAEA-CN-F-II, Kyoto, 1986.
19) T.K. Chu et al., Nucl. Fusion 26 (1986) 666.
20) F.X. Söldner et al., Phys. Rev. Lett. 5 (1986) 1137.
21) D. Van Houtte et al., Nucl. Fusion 24 (1984) 1485.
22) JT-60 team, Proc. 11th Int. Conf. Plasma Phys. Contr. Fusion, IAEA-CN-K-I-1, Kyoto, 1986.
23) K. Ushigusa et al., JAERI M 87-012, 1987.

24) F. Wagner et al., Phys. Rev. Lett. 56 (1986) 2187.
25) K. Uehara, J. Phys. Soc. Jpn. 53 (1984) 2018.
26) M.F. Xia and W.M. Wu, Plasma Phys. Contr. Fusion 29 (1987) 621.
27) J. Dawson, Phys. Fluids 4 (1961) 869.
28) M.J. Mayberry et al., Phys. Fluids 30 (1987) 2288.
29) M. Saigusa et al., same in ref. 12)
30) H. Kimura et al., same in ref. 10)
31) H. Kimura et al., in Proc. 14th European Conf. Plasma. Phys. Nucl. Fusion, Madrid. 1986.
32) A. Fukuyama et al., Computer Phy. Rep. 4 (1986) 137.

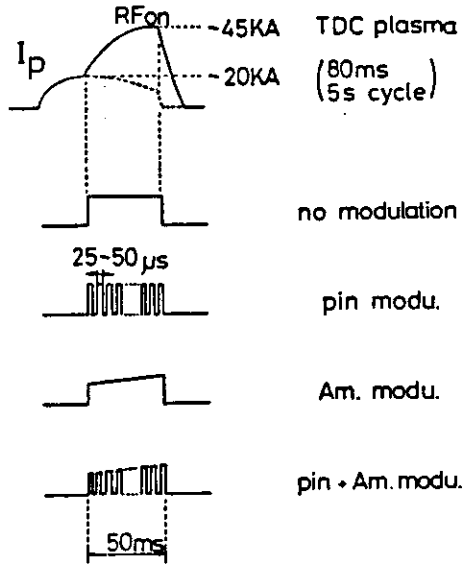

Fig. 1 LHRF Wave pattern in the aging process and the time behavier of TDC plasma

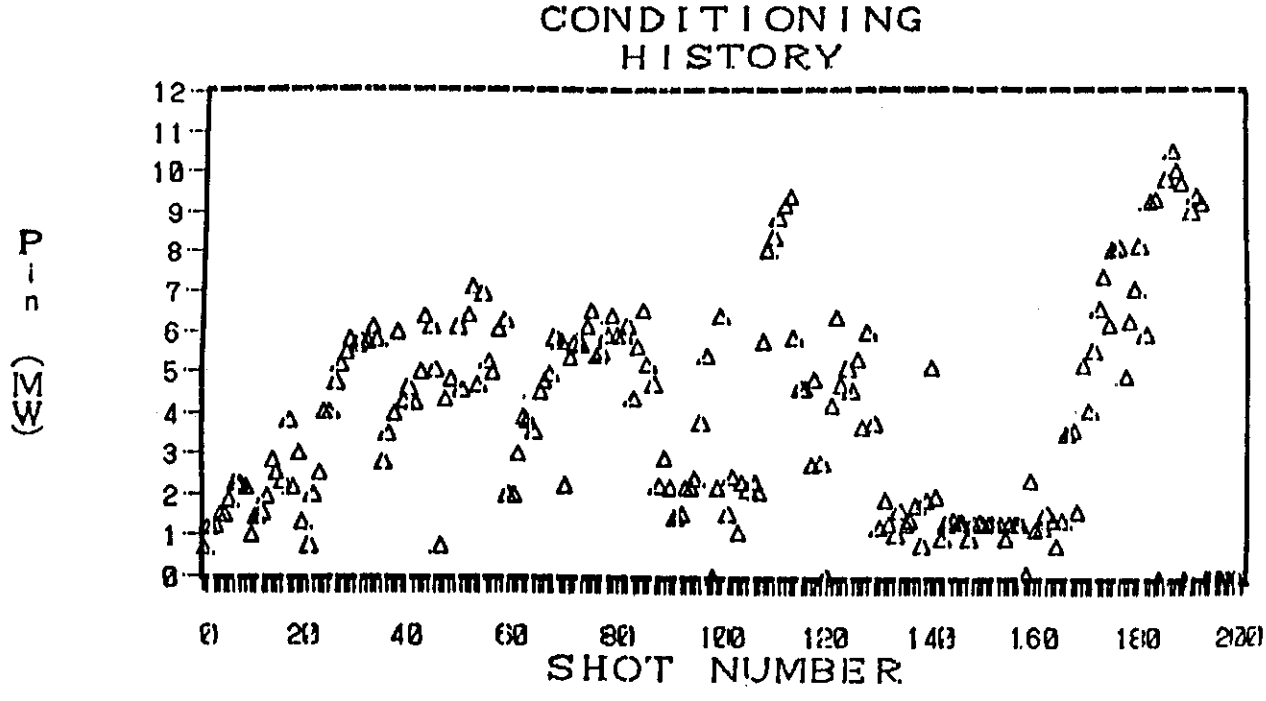

Fig. 2 LHRF conditioning history is shown against the shot number

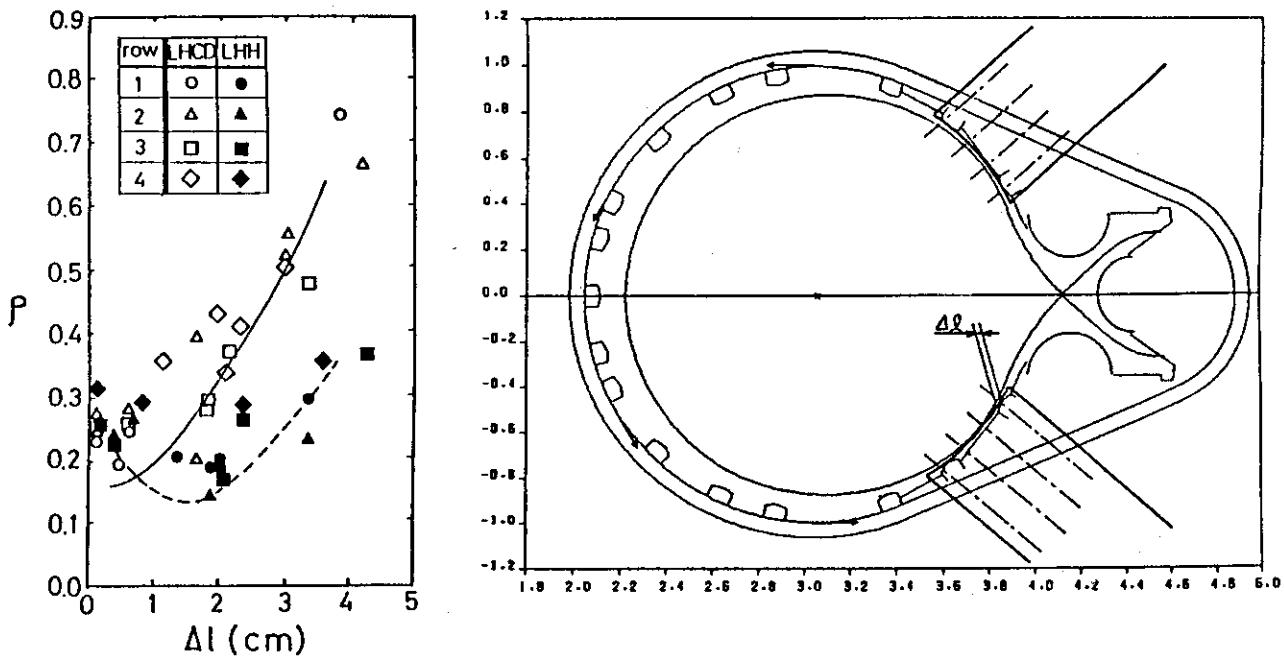

Fig. 3 Refrection coefficient vs the distance between plasma and the launcher, where $n_{es}=1\times10^{18}m^{-3}$, $\Delta L=0.5$ cm and $\lambda=0.5$ cm are assumed.

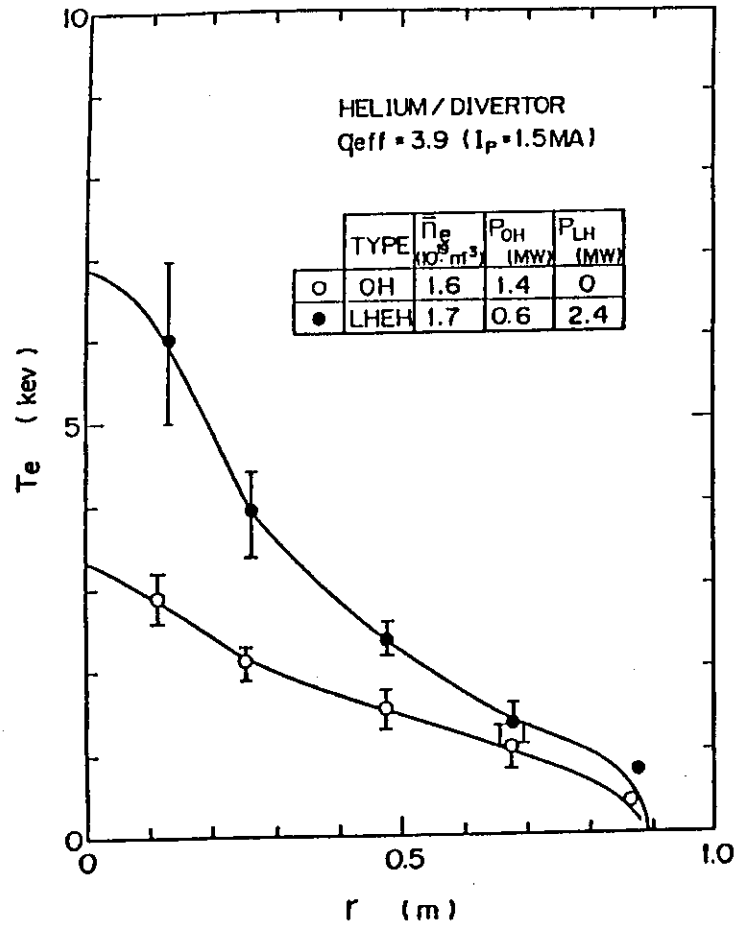

Fig. 4 Electron temperature profile when the maximum central electron temperature is obtained by LHEH, where $\bar{n}_e=1.7\times10^{19}m^{-3}$, $I_p=1.5$ MA.

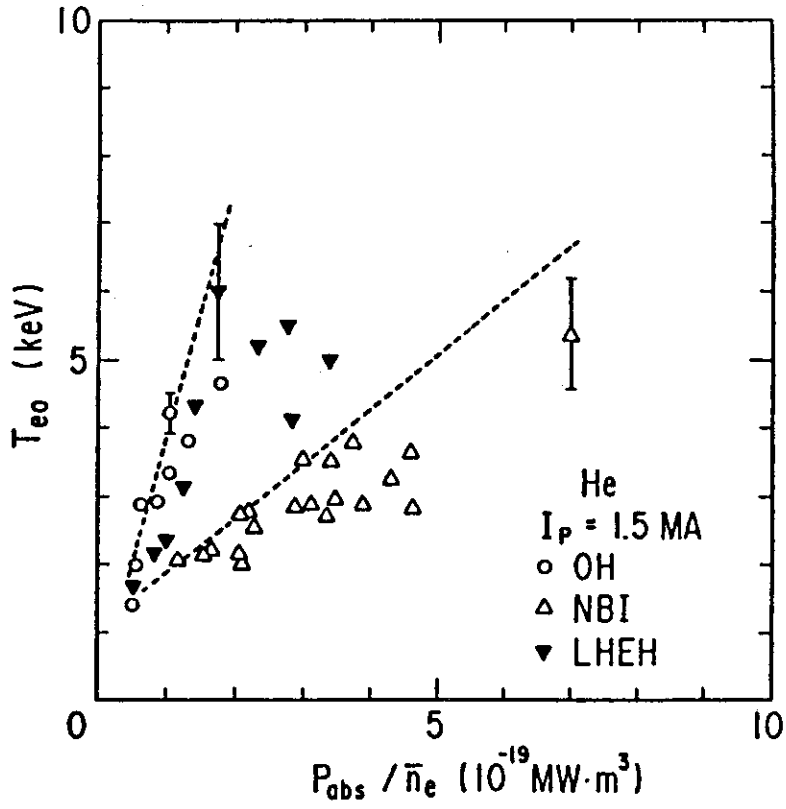

Fig. 5 Central electron temperature T_{e0} vs $P_{abs}/\bar{n}$, where the absorption power of LHRF is torus input P_{LH}.

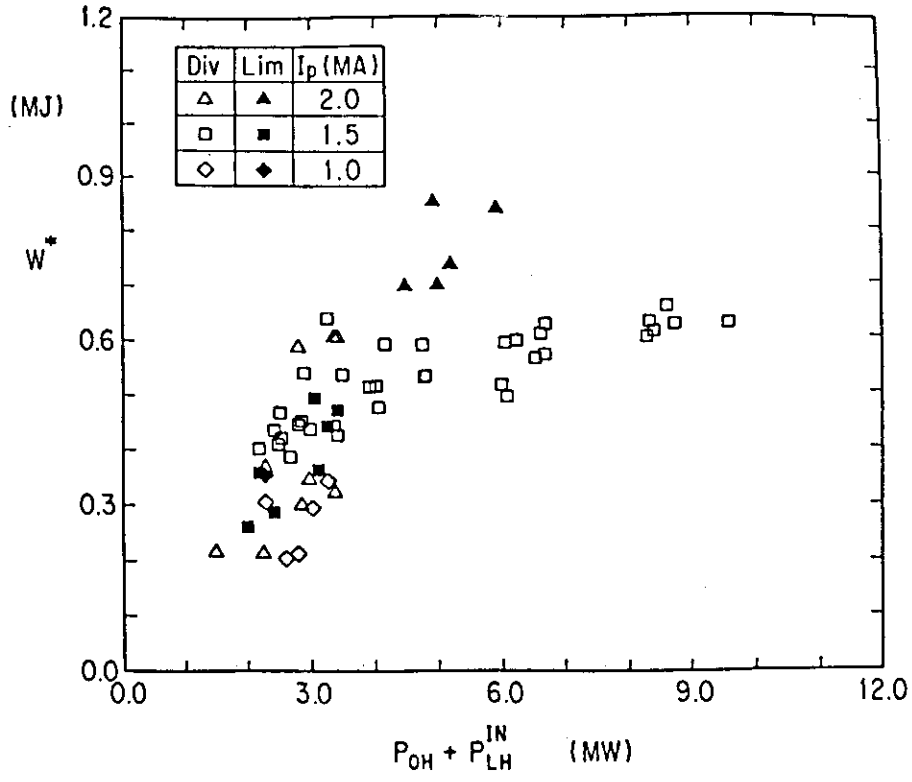

Fig. 6 Stored energy W^* against P_{abs} in LHEH putting I_p as a parameter. The value of W^* does not saturate at I =2.0 MA.

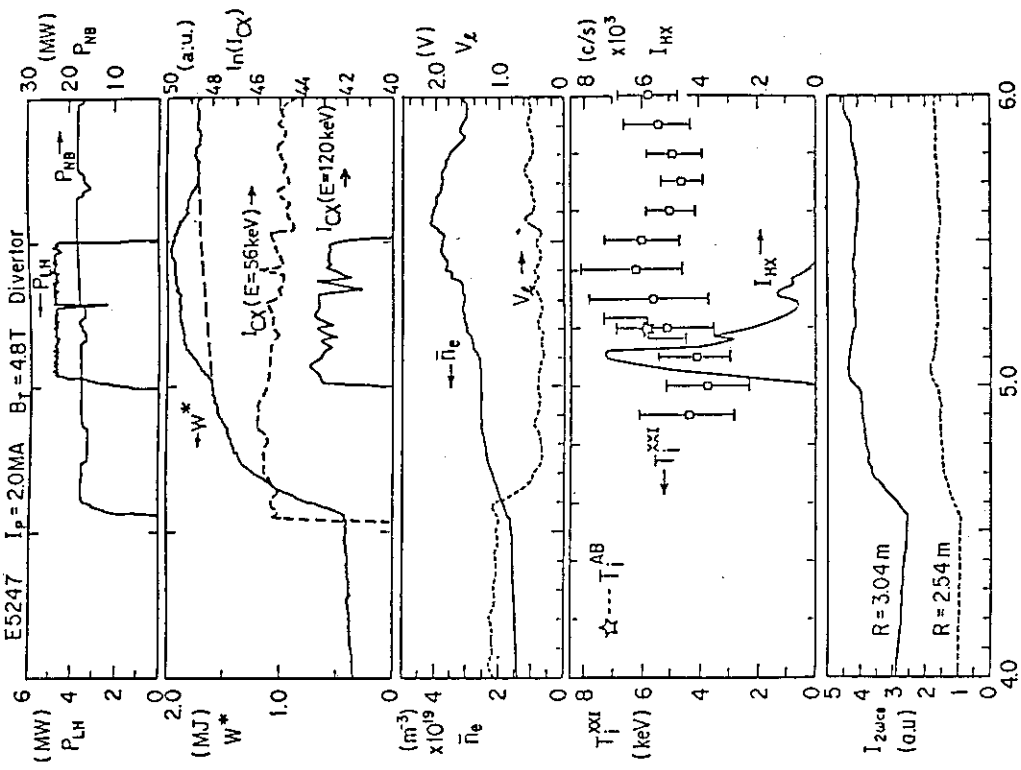

Fig. 8 Simultaneous injection of NBI and LHRF. Time behaviour of input power of both P_{LH} and P_{NB}, W^*, $\bar{n}_e$, ion temperature by titanium XXI line T_i^{XXI}, active beam T_i^{AB}, hard X ray signal and electron cyclotron emission ($2\,\omega_{ce}$) are shown, respectively.

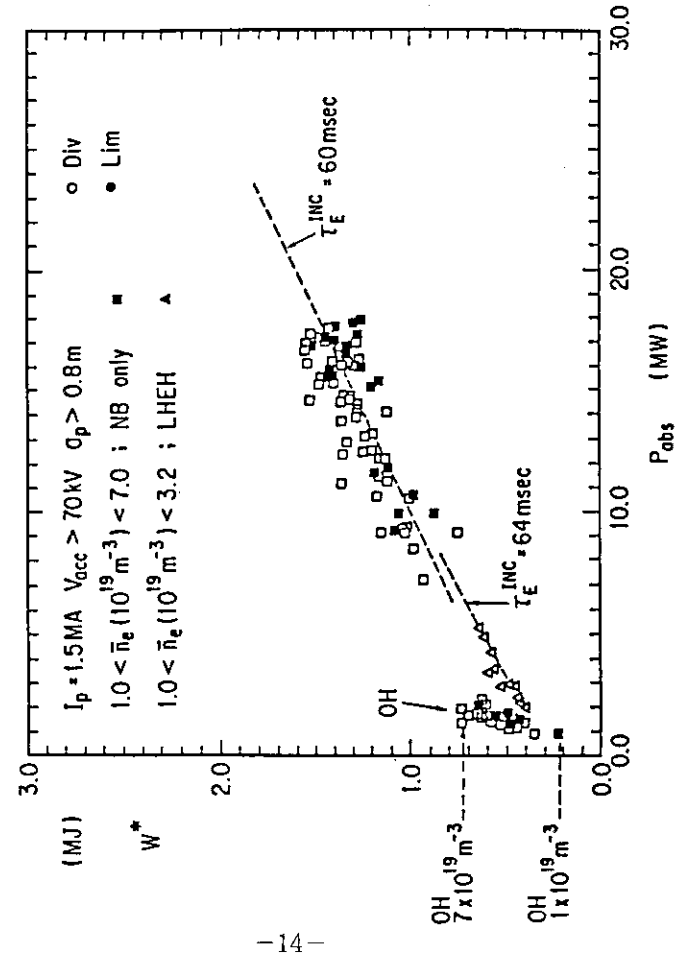

Fig. 7 Comparison of W^* and τ_E in LHEH case with NBI case.

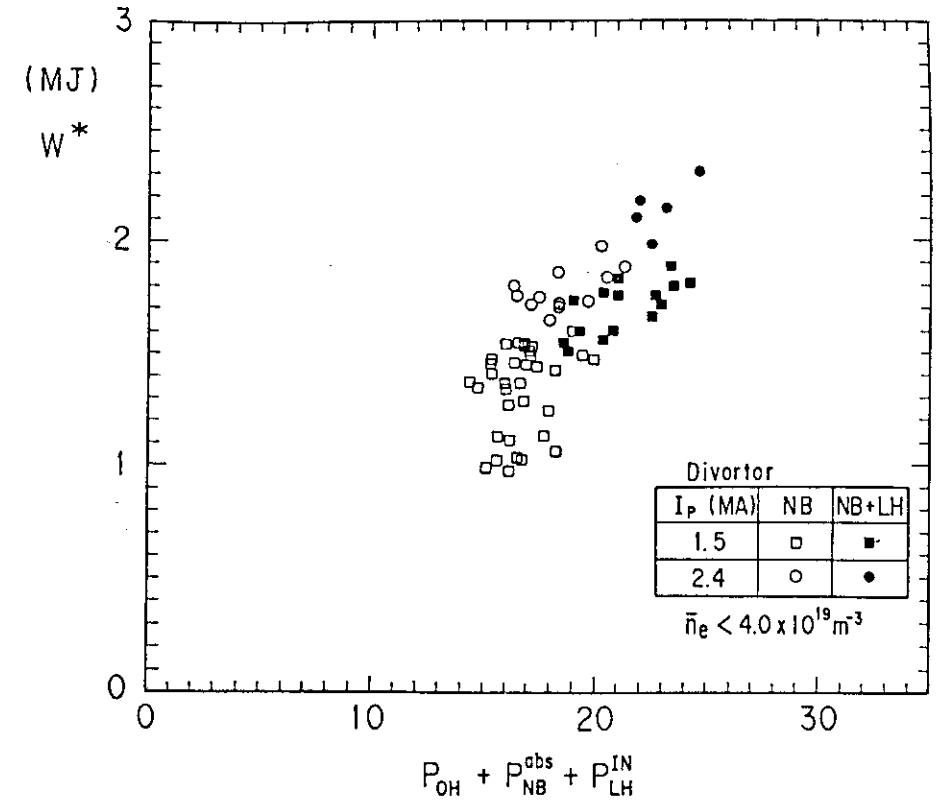

Fig. 9 The value of W^* in NBI+LHEH case is shown against $P_{OH}+P_{NB}+P_{LH}$.

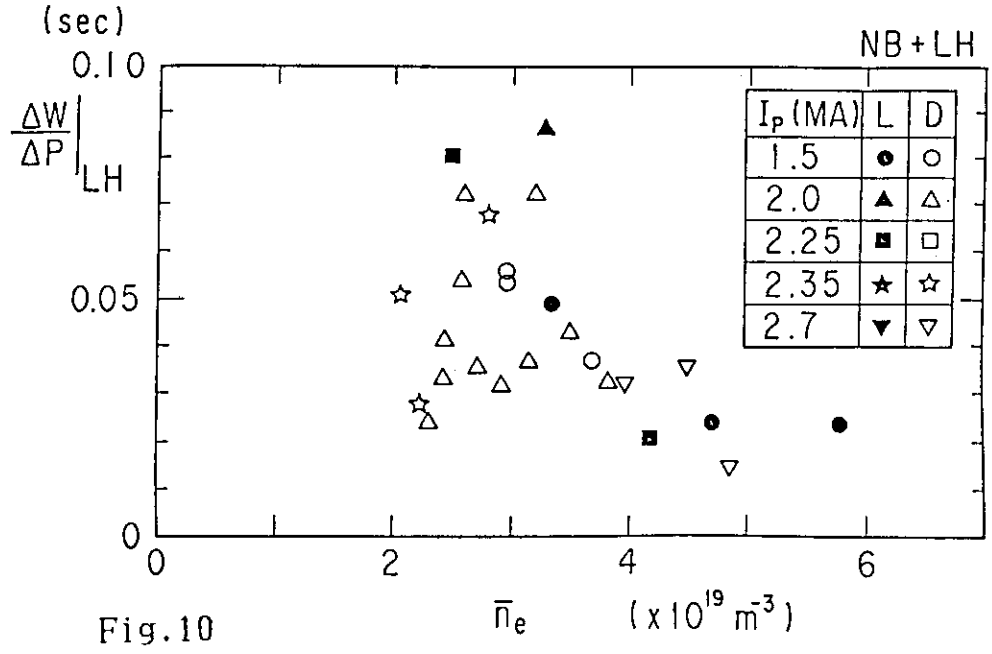

Fig.10

Fig. 10 Incremental energy confinement time ($\Delta W/\Delta P$) by LHRF in NBI+LHRF case is shown against $\bar{n}_e$.

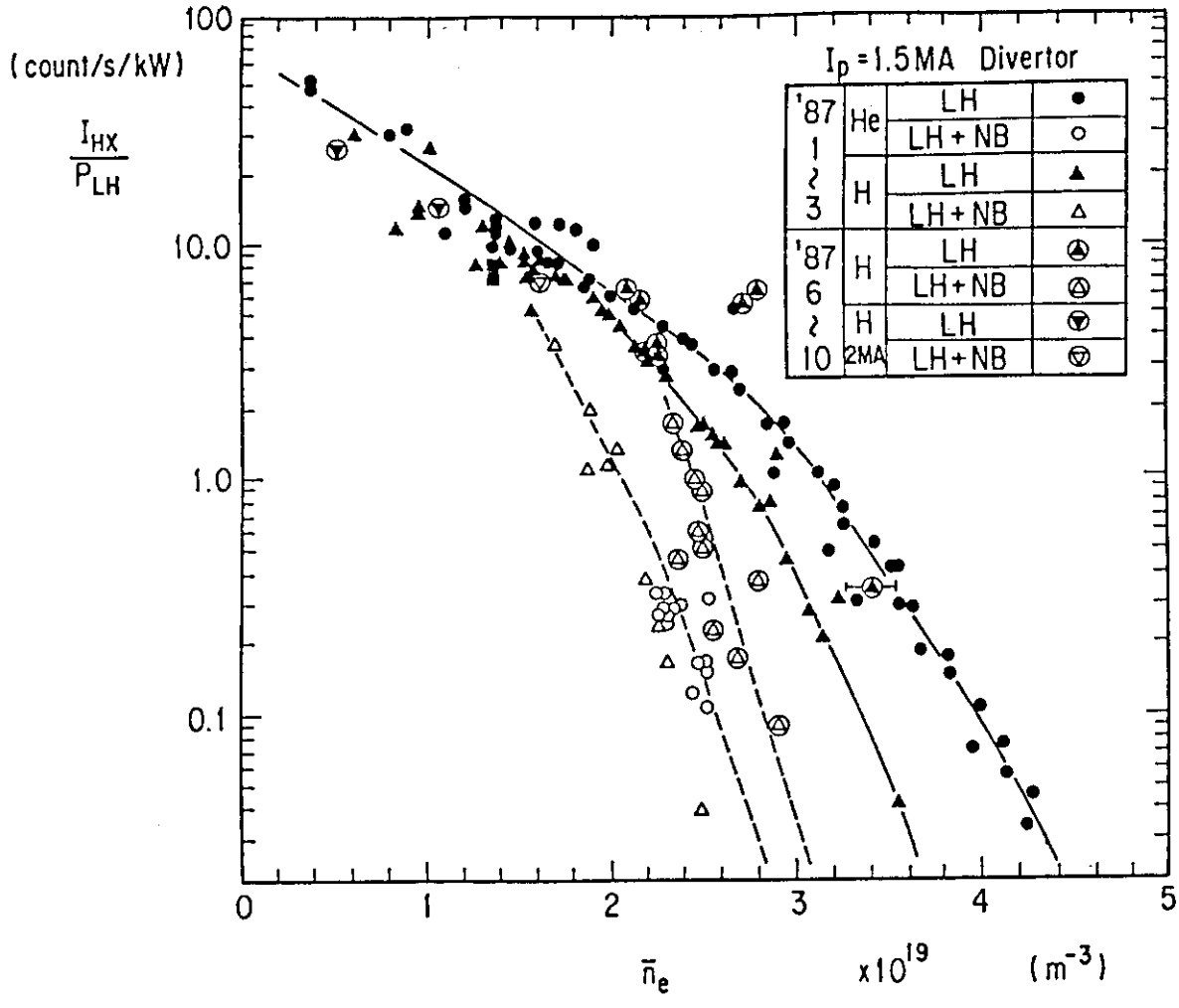

Fig. 11 Signal intensity of hard X ray I_{HX} normalized by P_{LH} is shown against $\bar{n}_e$. In NBI+LHEH case, I_{HX}/P_{LH} decreases suddenly at $\bar{n}_e=2.5\times10^{19}m^{-3}$.

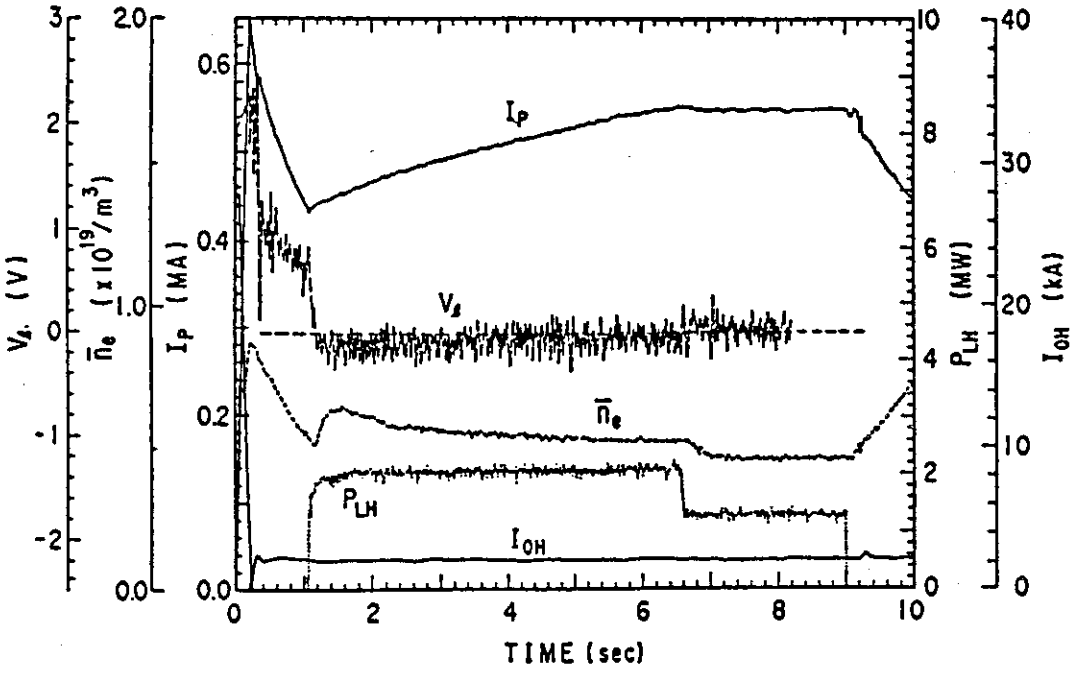

Fig. 12 Typical current ramp-up shot in JT-60.

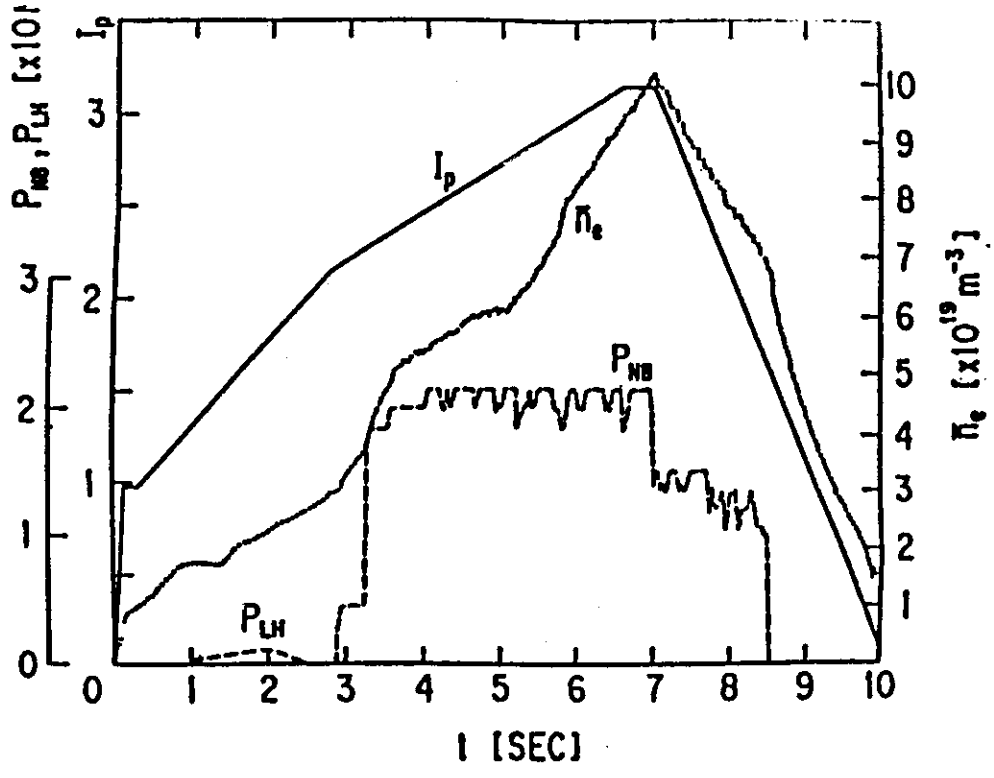

Fig. 13 High plasma current formation of 3.25 MA by assistance of LHRF ramp-up. In this short, about 0.6 volt·sec is saved by LHRF.

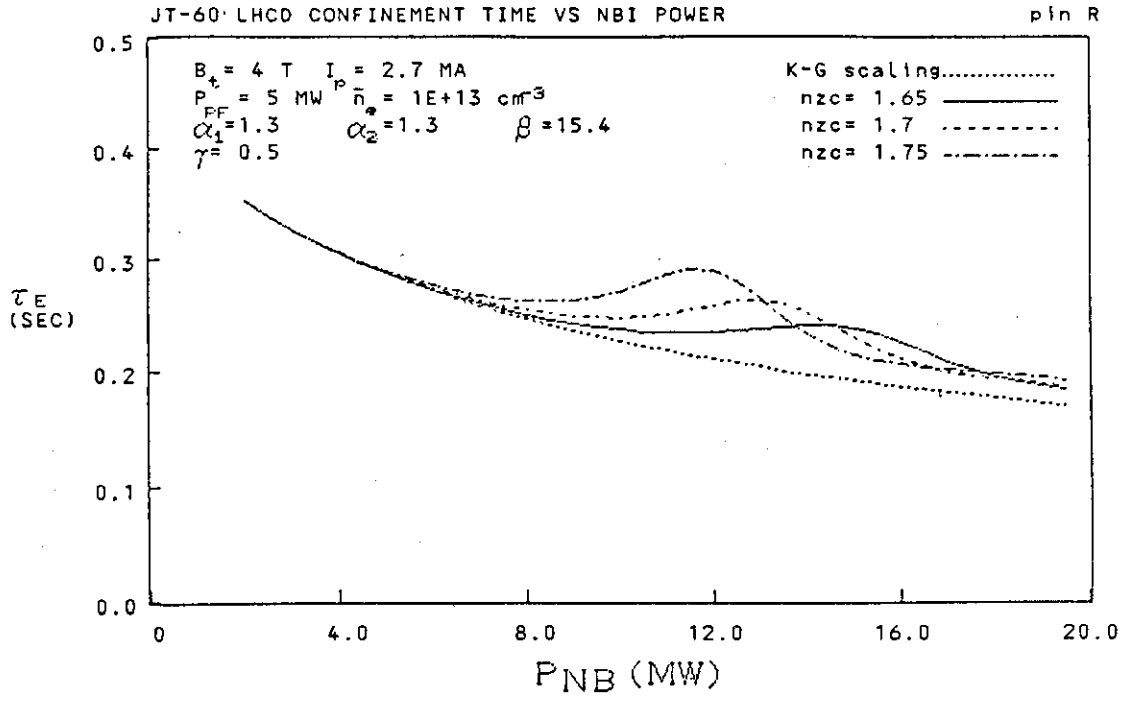

Fig. 14 Simulation of the improvement of τ_E in JT-60 LHCD and NBI by the pinch effect. The value of τ_E is improved when electron temperature is in a certain value, where P_{NB} is the function of the electron temperature.

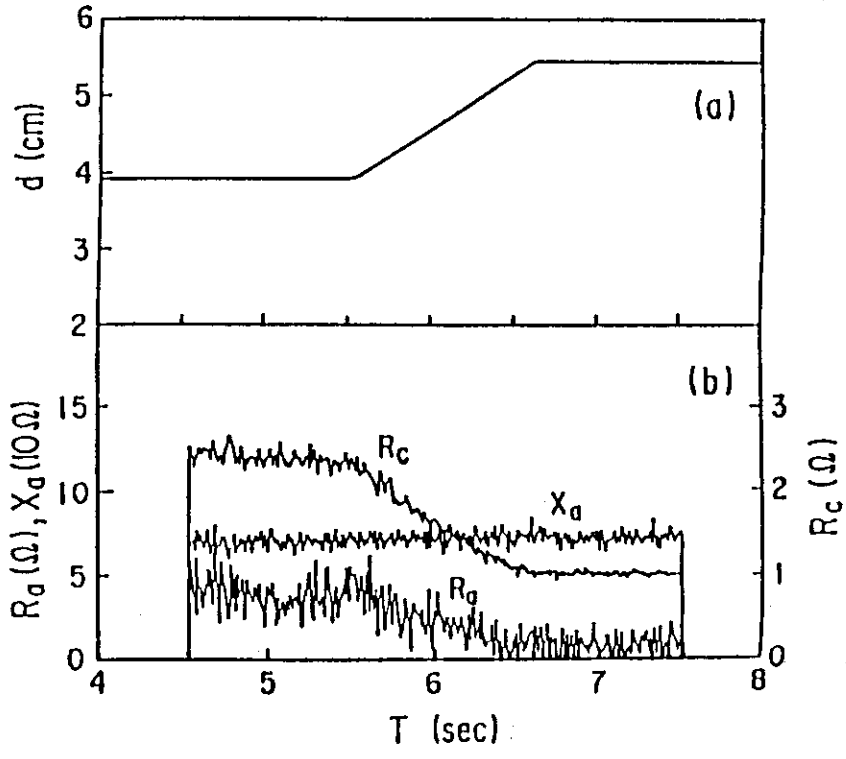

Fig. 15 Data for the prediction of stub position, where R_c is real resistance, X_a is imaginary part and R_a is obtained impedance.

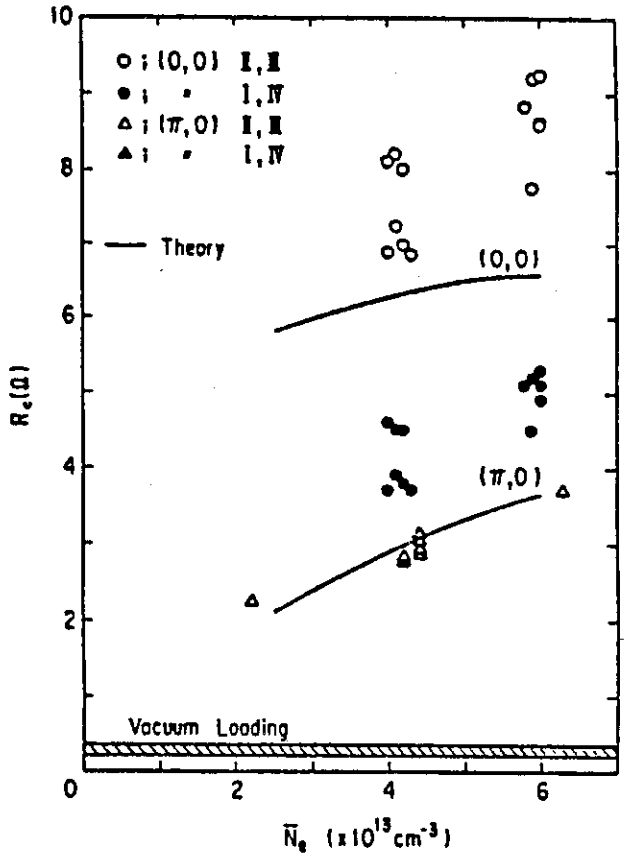

Fig. 16 Antenna loading resistance R_c against $\bar{n}_e$ in (0,0) and (π,0) case.

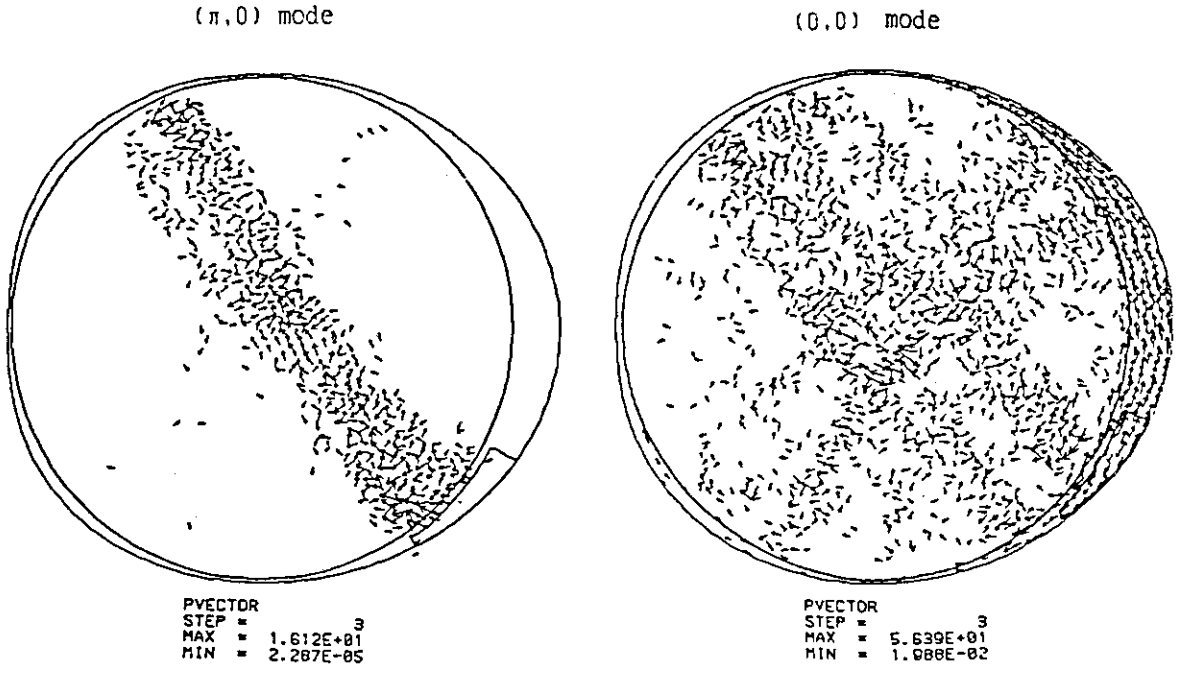

Fig. 17 Poynting vector and power deposition profile in the poloidal cross section estimated by two domensional kinetic wave theory in (0,0) and (π,0) phasing.

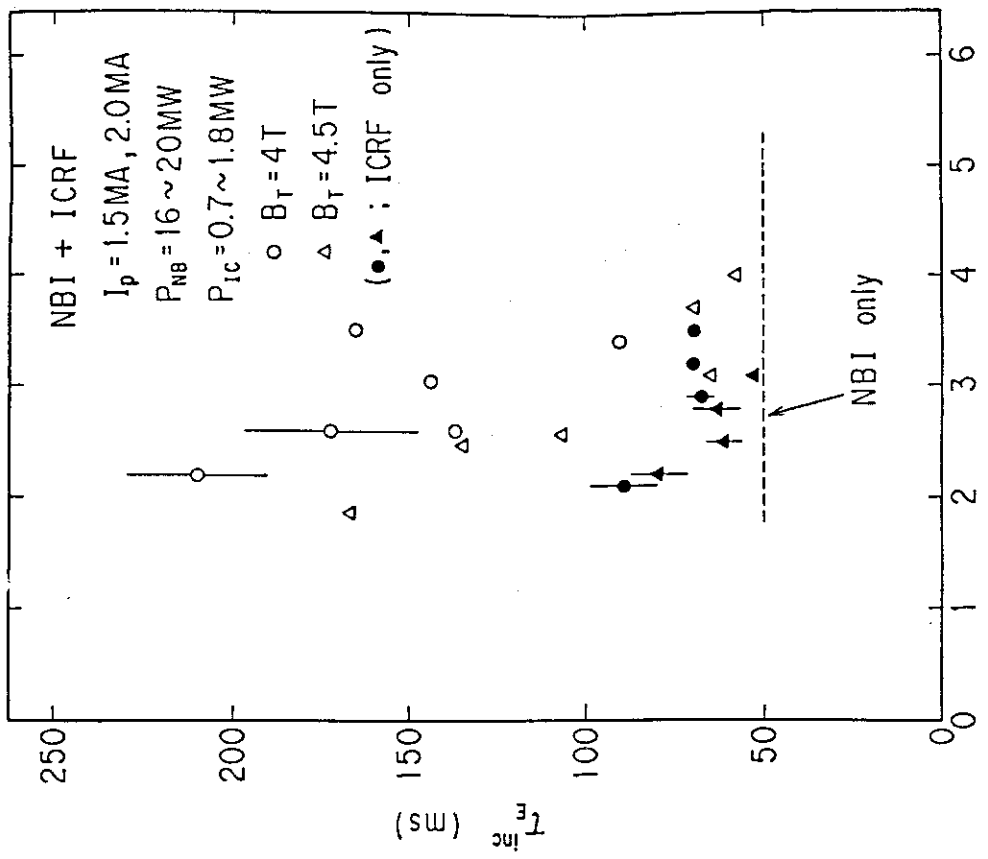

Fig. 19 The value of τ_E^{INC} is shown against $\bar{n}_e$ in the beam acceleration by ICRF.

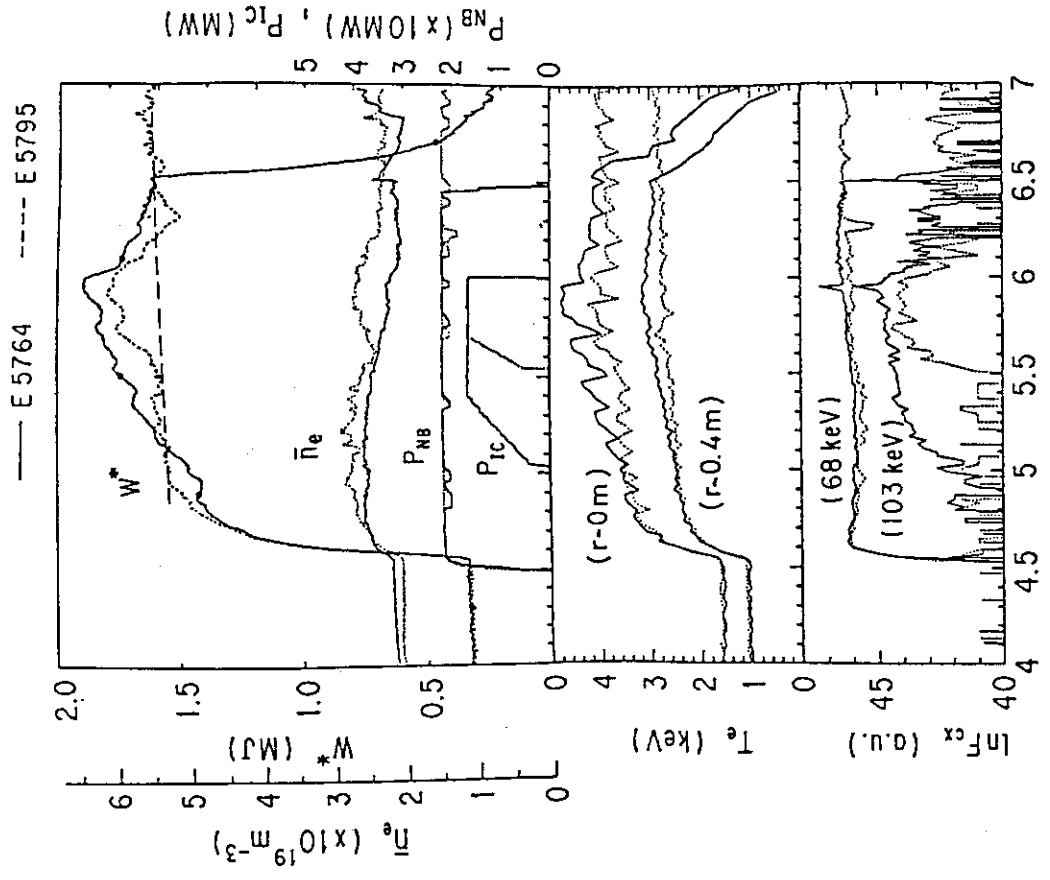

Fig. 18 Data on beam acceleration by ICRF including W^*, $\bar{n}_e$, P_{NB}, P_{IC}, T_e by ECE and the neutral flux with 68 keV and 103 keV by charge exchange analyser.